Journal of Engineering and Sustainable Development
Vol. 28, No. 05, September 2024
https://jeasd.uomustansiriyah.edu.iq/index.php/jeasd
ISSN 2520-0917
Research Article
https://doi.org/10.31272/jeasd.28.5.12

Revisiting the Code Design Equations for Concrete Columns Reinforced with GFRP Bars

Mohamed Qassim Kadhim[1*], Hassan Falah Hassan[2]

[1, 2]Civil Engineering Department, College of Engineering, Mustansiriyah University, Baghdad, Iraq

[1]https://orcid.org/0009-0007-0037-6453,
[2]https://orcid.org/0000-0003-4610-0560)
[*]Email: mohamedq1992@uomustansiriyah.edu.iq

Article Info

Received 07/07/2023
Revised 16/08/2024
Accepted 17/08/2024

Abstract

Over the previous three decades, researchers have dedicated significant efforts towards the advancing of glass fiber-reinforced polymer (GFRP) bars, aiming to address the challenges arising from corrosion in traditional steel reinforcement bars. This study intended to find the most efficient relation to compute compression load capacity for concrete columns of circular sections reinforced with GFRP through surveying equations from previous research and comparing the relations of the most popular GFRP codes (JSCE, AS, CSA, and ACI). The statistical analysis of the equations depends on a comparison of practical and theoretical load capacities, Young's modulus, compressive concrete strength, ratios of longitudinal and both types of transverse reinforcement, spirals, and hoops. The results of CSA and AS were close to each other, and they were better than those of JSCE and ACI regarding being efficient, safe, and consistent. In addition, JSCE demonstrated a high level of conservative in all the studied parameters, followed by the ACI, while the CSA and AS showed very low conservative rates. Furthermore, the AS showed superiority in all the studied parameters. In terms of statistical metrics, the AS exhibited a very low error rate. It was concluded that the AS relation is the most efficient and superior relation for computing the axial load carrying capacity (ALCC) of all the studied parameters, followed closely by the CSA code equation, and with a slightly larger margin, the ACI code equation then JSCE code equation with a slightly very large margin.

Keywords: GFRP Bars; Code Design Equations; Axial load; Calculated load; Experimental load; Hoops; Spirals

1. Introduction

To enhance the tensile strength of concrete members, steel bars are commonly incorporated as reinforcement, as concrete itself exhibits weakness in tension despite its strength in compression [1]-[3]. The utilization of fiber-reinforced polymer (FRP) bars as reinforcement for concrete members has witnessed a significant increase in recent decades, primarily driven by concerns regarding the corrosion problem associated with steel bars [4]. FRP bars have gained popularity due to their inherent corrosion resistance, effectively addressing the corrosion problem associated with steel bars. Additionally, FRP bars offer the advantage of higher tensile strength per unit weight compared to steel bars [5]. However, it is widely acknowledged that the compressive strength of FRP bars ranges between 36% and 77% of their tensile strength. Furthermore, the modulus of elasticity (stiffness) of FRP bars in compression ranges from 65% to 97% of their stiffness in tension [6]-[13]. The reduced compressive strength and stiffness in FRP bars can be attributed to the micro-buckling phenomenon exhibited by individual fibers. This micro-buckling leads to premature failure of FRP bars when subjected to compressive loads [14]. Consequently, previous design standards imposed restrictions on the utilization of FRP bars in compression members or the compression zone of flexural members [15], [16]. Previous American standards, such as ACI: 440.1R-06 [17] and ACI 440.15 [18], did not permit the utilization of FRP in compression members. In contrast, the Japanese standard (JSCE 1997 [19]) took a bolder approach by allowing the use of FRP in compression members more than 25 years ago. However, it overlooked the contribution of longitudinal bars to the ALCC of the compression member and instead focused on the type of transverse reinforcement as a determinant for predicting the ALCC. Ongoing research focuses on the

utilization of FRP bars for reinforcing compression members in structural concrete [20]-[22]. Previous studies have indicated that GFRP bars contribute approximately 3% to 14% of the total axial load sustained by GFRP bar-reinforced concrete columns, while steel bars contribute around 12% to 30% of the total axial load in steel bar-reinforced concrete columns [11]-[17], [20]-[30]. Several scholarly investigations have examined the performance of slender concrete columns reinforced with FRP bars. These studies have observed that, when subjected to axial compression, FRP bar-reinforced columns exhibited comparable load-bearing capacities to those reinforced with steel bars [11]-[17], [20]-[31]. However, in the case of eccentrically loaded columns reinforced with FRP bars, some studies have suggested disregarding the contribution of the FRP bars [32], [33]. Several studies have shown that neglecting the role of FRP bars in the compression zone can lead to an underestimation of the ALCC of eccentrically loaded FRP bar-reinforced concrete columns, with potential underestimations of up to 27% [34]-[39]. Additionally, recent research has investigated the performance of FRP bar-reinforced seawater sea sand concrete in various harsh environments, demonstrating no notable deterioration in the structures even after prolonged exposure [40], [41]. Previous research has made notable contributions to enhancing our understanding of the performance of concrete columns reinforced with FRP bars. However, there remains a lack of consensus regarding the specific contribution of FRP bars, when used as longitudinal reinforcement, to the axial load capacity of concrete columns [42]. Consequently, extensive research has prompted revisions to the design and implementation standards for FRP in compression members. These revisions have been implemented through the Australian standard (AS-3600 [43]), followed by the Canadian standard (CSA S807-19 [44]), and the American standard (ACI 440.11-22 [45]). Notably, the primary discrepancy among these modern standards lies in whether the contribution of longitudinal bars is disregarded or taken into account when estimating the ALCC of the compression member.

2. Research Significance

Due to the numerous advantages of FRP, guidelines often tend to be conservative, thereby increasing the cost of structure construction and hindering the widespread use of FRP. This research focuses on GFRP due to its unique advantages over other types, making it a fertile ground for research in terms of its implementation in compression members. Furthermore, modern code equations have not been thoroughly studied, compared, and evaluated for their safety, consistency, and cost. This study aims to evaluate the ALCC of columns reinforced with GFRP bars and spirals or hoops by using code equations. Experimental data from previous studies were collected, and the validated equations were those of ACI, CSA, AS, and JSCE codes. The code equations were assessed by comparing experimental and theoretical loads based on GFRP stiffness, compressive strength, types of reinforcement (hoops and spirals), and longitudinal and transverse reinforcement ratios. Several statistical measures were used to evaluate these equations and determine the amount of error and deviation from the ideal behavior for each equation.

3. Experimental Database

A collection of 165 GFRP-reinforced concrete (GFRP-RC) columns (100 specimens were circular and the rest were square) subjected to concentric compression load were adopted to investigate the performance of them under compression load and examine several codes of design [21], [23], [37], [46]-[69]. Specimens had long and short columns. Table 1 lists axial compression design parameters. The ratio of longitudinal reinforcement for both column shapes ($\rho_{fl} = n \times A_b/A_g$), where n is the longitudinal reinforcements bars' number, A_b is the GFRP bar's area, and A_g represents the gross sectional area, it was ranged between (0.37- 4.1) %. The transverse reinforcement ratio for both column shapes ($\rho_{ft} = 4 \times A_{ft}/D_c \times s$), where A_{ft} means the GFRP transverse reinforcement bar's area, D_c represents the diameter of the core, and s means the spacing among the spirals or hoops, between 0.38% and 5.94%. E_{fl} is the modulus of elasticity for longitudinal reinforcement, ranging from 42 GPa to 66 GPa. $E_{ft}$is modulus of elasticity for the transverse reinforcement, between 42 and 76 GPa. f_{ful} represents the tensile strength of the longitudinal reinforcement, from 574 to 1,600 MPa. In addition, f_{fut} is the tensile strength of the transverse reinforcement, it was between 650 MPa and 1,700 MPa.

4. Maximum Axial Loads Carrying Capacity of GFRP-RC Columns

It is important to remember that the contribution of concrete to the analytically determined axial load capacity of GFRP bar-reinforced concrete columns is not the same across all code equations. Therefore, the differences in the values of P_o for GFRP reinforced concrete columns result from the calculation or ignoring of the effect of the longitudinal bar in the different equations to know the contribution of the longitudinal bar ($P_{bar,FRP}$) in addition to the difference in the factors used in other equations when calculating the effect of the longitudinal bar. As known, the compressive strength of the FRP bar is much smaller than its tensile strength, so its performance under compressive loads is different. So, previously ACI 440.1R-06 and ACI 440.1R-15 [17],[18] suggested that FRP should not be employed as a longitudinal reinforcement in columns. while CAN/CSA S806-12 [15] and JSCE 1997 [19] permit using FRP in reinforcing columns longitudinally. they saw that the effect of the FRP bars should not taken into consideration in the evaluation of the ultimate ALCC of FRP bar-reinforced concrete columns. Furthermore, the JSCE 1997 [19] recommendation relies on transverse reinforcement in the ALCC estimation equations and considers whether this reinforcement is spiral or tie types, ignoring the effect of longitudinal bars. Using the recommendation in JSCE 1997 [19], (1. a and/or 1. b) can be used to predict the maximum ALCC of FRP bar-reinforced concrete columns.

$$P_o = 0.85 f'_c A_g/\gamma_b \quad (1.\text{ a})$$

$$P_o = (0.85 f'_c A_e + 2.5 E_{sp}\varepsilon_{fspd} A_{spe})/\gamma_b \quad (1.\text{ b})$$

Table 1. Design parameters of the database columns tested under axial compression.

Number of columns	Total database					
	165					
	Shape	Min	Max	SD	M	COV (%)
$D\ (mm)$	Circular	125	305	55	260.4	21.1
	Square	125	350	67	179.2	37.4
$D_c\ (mm)$	Circular	112	240	45.8	197.9	23.1
	Square	98	284	58.5	128.1	45.7
$A_g\ (mm^2)$	Circular	12271.8	73061.7	20296.5	55591.1	36.5
	Square	15625	122500	32916.91	36750	89.6
R (mm)	Circular	62.5	152.5	27.5	130.2	21.1
	Square	88.4	247.5	47.3	126.7	37.4
L (mm)	Circular	500	2500	396.9	1220.1	32.5
	Square	500	1200	256.3	733.8	34.9
L/R	Circular	5.6	16.4	2.2	9.3	23.3
	Square	4.2	11.3	1.9	6.0	31.6
ρ_{fl} (%)	Both shape	0.37	4.10	0.67	1.92	34.68
f_{ful} (MPa)	Both shape	574	1600	241.3	1045.5	23.08
E_{fl} (MPa)	Both shape	42000	66000	7373.17	51322.73	14.37
ρ_{ft} (%)	Both shape	0.38	5.94	1.05	1.83	57.28
f_{fut} (MPa)	Both shape	650	1700	222.16	1044.84	21.26
E_{ft} (MPa)	Both shape	42000	76000	6914.92	51315.15	13.48
f'_c (MPa)	Both shape	15.10	85	14.49	37.87	38.26

* Min., Max., SD, μ, and COV represent minimum value, maximum value, standard deviation, mean value, and coefficient of variation, respectively.

where A_g represents the concrete cross-sectional area (mm^2), A_e means the concrete cross-sectional area confined by spirals, A_{spe} is the equivalent spiral's cross-sectional area ($= \pi d_{sp} A_{sp}/s$), d_{sp} is the diameter of the concrete section surrounded by spiral reinforcement, A_{sp} is the cross-sectional area of spiral reinforcement, E_{sp} is the young's modulus of spiral reinforcement (E_{ft}), ε_{fspd} represent the design spiral strain at the ultimate limit condition, 2000×10^{-6}, γ_b means the member factor, it is 1.3, s represent the spacing of spiral. JSCE 1997 [19] declared that for members subjected to compression load, the ultimate limit of compression load capacity P_o can be computed by (1. a) when ties are adopted and either (1. a) or (1. b) whatever gives the largest value when spiral reinforcement is adopted. However, many studies found that omitting the effect of FRP longitudinal bars in compression may cause a large difference between the evaluated ALCC of FRP-reinforced columns and the experimental value [21],[28],[30]. Therefore, due to the advancement of knowledge in the use of fiber in compression members, the code recommendations have been updated in several countries gradually. This occurred for the first time in the Australian code recommendation AS-3600 [43], which stipulated not neglecting the effect of longitudinal bars when calculating the maximum ALCC of the concrete columns. It also took into account the influence of the stiffness of this bar in the ALCC of the concrete column, considering an axial strain value of the longitudinal bar at the beginning of the microcracks in the plastic stage of the concrete equal to 0.0025. So, (2) can be used to predict the maximum ALCC of FRP bar-reinforced concrete columns according to AS-3600 [43]:

$$P_o = 0.85 f'_c (A_g - A_f) + f_{frp} \times A_f \quad (2)$$

where A_f is the overall GFRP longitudinal bars' cross-sectional area of, $f_{frp} = \varepsilon_f \times E_f$ where $\varepsilon_f = 0.0025$ and represents an axial strain of the longitudinal FRP bar, and E_f is the modulus of elasticity of the longitudinal bar. In addition, the recommendation of the Canadian code (CSA S807-19 [44]) was similar to that of the Australian code (AS-3600 [43]) according to the same principle, which is not to neglect the effect of the longitudinal bar when calculating the maximum ALCC of the concrete columns with a difference in the axial strain value of the longitudinal bar, ε_f, which is equal to 0.002, as shown in (3):

$$P_o = 0.85 f'_c (A_g - A_f) + f_{frp} \times A_f \quad (3)$$

Finally, last year a new American code (ACI 440.11-22 [45]) was issued specialized in the use of GFRP in compression members, but although it allowed the use of GFRP in these compression members, it neglected its effect when calculating the maximum ALCC of the concrete columns, as shown in (4):

$$P_o = 0.85 f'_c A_g \quad (4)$$

The commentary of the code in clause (R22.4.2.2) was to state "GFRP compression reinforcement, while permitted, will not contribute significantly to the axial capacity of the cross-section. The calculation of nominal axial strength may be simplified by assuming that GFRP reinforcement in compression has the same stiffness and strength as the surrounding concrete and that P_o may be calculated using the gross area of concrete and f'_c". Several studies have shown that effectively neglecting the contribution of GFRP reinforcement in compression in this manner is conservative [27],[29],[47],[70-72]. It is worth noting that the targeted American code (ACI 440.11-22 [45]) in this statistical study is

specifically focused on GFRP, while the other targeted codes in this study (AS-3600 [43], CSA S807-19 [44], and JSCE 1997 [19]) specialize in all types of fibers. To reinforce the research idea, specimens were selected that were fully reinforced longitudinally and transversally with GFRP to align with the code recommendation, while other types of fiber reinforcements, such as basalt-FRP (BFRP), aramid-FRP (AFRP), and carbon-FRP (CFRP), were neglected. The ACI 440.11-22 [45] initially dedicated its recommendation to the use of GFRP only due to the extensive research available for this type in the field, while other types require further future studies to provide individual recommendations for each. In addition to the unique advantages of GFRP over other fiber reinforcement types that make it the first type recommended by the code for compression members, the remaining types are still subject to study.

5. Evaluation of the Codes Equations

5.1. General Performance

In this research, the relations of codes were tested in this investigation by analyzing a large body of available experimental data. The specimens of reinforced concrete columns with GFRP bars, totaling 165 specimens, were collected from 27 previous studies. The description of the specimens includes the specimen's name, specimen shape (circular or square), specimen dimensions, longitudinal and transverse reinforcement ratio, and the shape of the transverse reinforcement (spiral or hoop). It also includes the tensile strength of the longitudinal bars, the modulus of elasticity of the longitudinal bars, and the compressive strength of the concrete, as referred to in [21, 23, 37, 46-69]. It should be noted that the type of longitudinal and transverse reinforcement material is GFRP. The experimental load, which was used to calculate the experimental load-to-theoretical load ratio according to the four codes for all specimens, was compiled from the 27 references mentioned earlier.

The MEAN results for the experimental load-to-theoretical load ratio for ACI 440.11-22 [45], CSA S807-19 [44], AS-3600 [43], and JSCE 1997 [19] were 1.11, 1.07, 1.06, and 1.45, respectively. The SD results for the experimental load-to-theoretical load ratio for ACI 440.11-22 [45], CSA S807-19 [44], AS-3600 [43], and JSCE 1997 [19] were 0.20, 0.19, 0.18, and 0.27, respectively. The COV results for the experimental load-to-theoretical load ratio for ACI 440.11-22 [45], CSA S807-19 [44], AS-3600 [43], and JSCE 1997 [19] were 18.37%, 17.60%, 17.49%, and 18.35%, respectively. The analytically expected ALCC, P_o, was found by either using (1) JSCE 1997 [19], based predominately on the transverse reinforcement type (spirals or hoops), or using (2), according to AS-3600 [43] in which the value of axial strain of longitudinal bar ε_f was equal to 0.0025, or using (3), according to CSA S807-19 [44] in which the value of axial strain of longitudinal bar ε_f was equal to 0.002, or using (4), according to ACI 440.11-22 [45] in which the contribution of GFRP bar is neglected. The optimum line for each relation appears alongside the computed and measured axial load. The same number presents typical behavior. The relation between fewer scatters and better behavior is one where the most optimal line and the plotted data are closer to the perfect line. Four relations (f'_c, ρ_{fl}, E_{fl}, and ρ_{ft}) are shown to explain the ratio between the experimental and the computed axial loads by using the code relations for all examined columns. In addition, three mathematical measurements (Standard Deviation (SD), Mean (μ), and Coefficient of Variation (COV)) were adopted to determine the accuracy, safety, and consistency of the relations of the codes available using four codes (ACI 440.11-22 [45], CSA S807-19 [44], AS-3600 [43], and JSCE 1997 [19]). Mean (μ) is the midpoint between the wide continuum of P_o. More accurate outcomes can be obtained when the mean is close to one unit. The dispersion in P_o values was determined by SD. For concrete specimens with GFRP, a large SD means the expected ALCCs are within a wider value range of (smaller accuracy) and a lower SD means the adverse. The COV was then adopted to determine the dispersion (variation) of P_o values relative to the mean value as a percentage. when COV decreases, behavior tends to be more stable and less variable from the mean.

Performance criteria contain different types of performance matrices that are used to evaluate the reliability and accuracy of the code equations, such as:

Pearson's correlation coefficient (R), Nash–Sutcliffe efficiency index (NSEI), root-mean-square error (RMSE), a20index, mean absolute error (MAE), and mean absolute percentage error (MAPE). Furthermore, the following new engineering index, the a20-index, is proposed for the reliability assessment of the code equations. RMSE is a useful value to know because it gives us an idea of the average difference between the experimental data values and the predicted data values. The lower the RMSE, the more accurate the evaluation. Pearson's correlation coefficient R measures the variance that is interpreted by the equation, which is the reduction of variance when using the equation. R values range from -1 and values close to 1 indicate a strong positive correlation between the studied variables, while values close to -1 indicate a strong negative correlation. Meanwhile, a value closer to zero suggests a weak correlation or no correlation at all. These performance metrics are a good measure of the overall predictive accuracy. The NSEI and a20-index values, as well as Pearson's correlation coefficient, are close to one, indicating the high accuracy of the code equation. However, the errors such as MAE, MAPE, and RMSE must approach zero to satisfy the precision of the equation. The errors are used to compare the accuracy of several relations used to evaluate the ultimate ALCCs of GFRP-reinforced columns. If the errors are very slight, then the code relation should give precise outcomes. The most optimal slope of the line shows to which extent the behavior is consistent and meets the prediction or exceeds it for a specific parameter. The formulations used to calculate these performance indices are expressed in Equations (5) – (10) [73]-[75].

$$R = \frac{\sum_{i=1}^{N}(P_{exp.}-\overline{P_{exp.}})(P_o-\overline{P_o})}{\sqrt{\sum_{i=1}^{N}(P_{exp.}-\overline{P_{exp.}})^2((P_o-\overline{P_o})^2}} \quad (5)$$

$$MAE = \frac{1}{N}\sum_{i=1}^{N}\left|P_{exp.} - P_o\right| \quad (6)$$

$$MAPE = \frac{1}{N}\sum_{i=1}^{N}\left|\frac{P_{exp.}-P_o}{P_{exp.}}\right| \times 100 \quad (7)$$

$$RMSE = \sqrt{\frac{\sum_{i=1}^{N}(P_{exp.}-P_o)^2}{N}} \quad (8)$$

$$NS = 1 - \frac{\sum_{i=1}^{N}(P_{exp.}-P_o)^2}{\sum_{i=1}^{N}(P_{exp.}-\overline{P_o})^2} \quad (9)$$

$$a20 - index = \frac{m20}{N} \quad (10)$$

where N is the total number of collected specimen datasets, $P_{exp.}$ is the experimental load carrying capacity value, $\overline{P_{exp.}}$ is the mean of the experimental load-carrying capacity values, P_o is the predicted ALCC value, $\overline{P_o}$ is the mean of predicted ALCC values, and m20 is the sum of the ratios of the experimental values to the predicted values for all samples, divided by the number of samples, and the equation is considered safe and consistent if the values range from 0.8 to 1.2. If they fall outside these limits, the equation is either overly conservative and costly structurally, or its application leads to increased risks. Furthermore, an m20 value approaching 1 indicates that the equation is very safe and consistent, providing reasonable predictions. Performance matrices of code equations by the values of statistical indexes R, MAE, MAPE, RMSE, NSEI, and a20-index are presented in Table 2.

Table 2. Performance matrices of code equations.

Equation	R	MAE (KN)	MAPE (%)	RMSE (KN)	NSEI	a20-Index
ACI 440.11-22 [45]	0.9724	275.08	16.85	369.53	0.9264	1.1147
CSA S807:19 [44]	0.9756	229.44	14.72	323.48	0.9430	1.0699
AS-3600 [43]	0.9763	214.06	14.14	310.42	0.9474	1.0556
JSCE 1997 [19]	0.9724	595.60	31.60	738.42	0.7458	1.4489

It was observed that (2), in which the effect of GFRP bars is determined depending on their stiffness and the axial strain of longitudinal bar ε_f equal to 0.0025, is a more accurate and safe method to expect P_o than (3), in which the effect of GFRP bars is determined depending on the same principle but the axial strain of longitudinal bar ε_f equal to 0.002. Also, (4) is a more reliable and safer method to expect P_o than (1. a, 1. b), which adopted transverse reinforcement. The probable demonstrations for that contain the issue that despite the difference in the underlying principle between the two equations, where (4) disregards the influence of both longitudinal and transverse reinforcement and considers the specimen as a complete concrete section, while (1) relies solely on the contribution of transverse reinforcement and neglect the effect of the contribution of the longitudinal reinforcement, the contribution of transverse reinforcement does not significantly affect the value of the maximum ALCC. This is evident from the close convergence between the (1) and (4) in terms of the value of R. Furthermore, the clear explanation for the superiority of the (2) and the (3) successively over both the (1) and the (4) successively is that they take into consideration the contribution of the longitudinal bars in calculating the maximum ALCC of the column. The COV and SD are 17.49 and 0.18 respectively, when P_o is determined using (2), the relation of the Australian code (AS-3600 [43]). This permits more consistent results. By setting ε_f equal to 0.0025 when computing $P_{bar,GFEP}$, predictions for $P_{exp.}/P_o$ with = 1.06, which is very close to unity, were gained (Fig. 1). As shown in Fig. 1, the COV and SD are 17.6 and 0.19 respectively, when using the (3) available in (CSA S807-19 [44]), is adopted to determine $P_{bar,GFRP}$, resulting in smaller discrepant values of P_o. Furthermore, SD and COV in (4) are 0.2 and 1.11, respectively. Thus, the (2) that is available in AS presents more reliable expectations in a comparison of the codes (CSA, JSCE, ACI). This is a very small difference compared to (2) and (3), which yield very close results. In contrast, (1) shows SD and COV of 0.27 and 18.35, respectively. Moreover, (1) is very conservative with related to the use of GFRP in a compression member, as the experimental load to design load is 1.45, which is the highest among all the other code equations. The ALCC of GFRP reinforced columns were obtained from past research and put in a comparison with ALCC calculated using ACI 440.11-22 [45], CSA S807-19 [44], AS-3600 [43], and JSCE 1997 [19], respectively in Fig. 1. The trend line slope is 1.11 for the ACI, 1.07 for the CSA, 1.06 for the AS, and 1.45 for the JSCE. Also, the axial load was determined by adopting AS and CSA, and that is more in line with the experimental axial load. ACI, CSA, AS, and JSCE each found a COV for experimental axial load versus a predicted axial load of 18.37, 17.6, 17.49, and 18.35, respectively. AS and CSA are very close and they are the most accurate compared to ACI and JSCE. When comparing the AS relation to the others that were adopted, it was seen that it is the most precise in predicting the ALCC. Finally, the performance tests on concrete compression design practices revealed that AS-3600 [43] relation with appropriate factors of safety had better optimization, the second is CSA S807-19 [44] code, then ACI 440.11-22 [45] code, and the JSCE 1997 guidelines [19]. The AS-3600 [43] design equation and the CSA S807-19 [44] guidelines did better than the ACI 440.11-22 [45] code, which had some extreme values because they had fewer conservative columns. The JSCE 1997 [19] was not safe and had more penalty points than the other design equations because it is more conservative.

5.2. Modulus of Elasticity (Young's Modulus)

Young's modulus has a large effect on the ALCC of GFRP-reinforced concrete columns. $P_{exp.}/P_o$ vs. the E_f and the most optimal line trendlines of the database are plotted in Fig. 2. $P_{exp.}/P_o$ increases when Young's modulus increases. The best lines of ACI, CSA, AS, and JSCE have a slope of 1E-5, 1E-5, 9E-6, and 1E-5, respectively. Also, the square Pearson's correlation coefficient for the ACI, CSA, AS, and JSCE have 0.1508, 0.1388, 0.1327, and 0.1512, respectively. Therefore, CSA gives higher consistency in terms of E_f in terms of safety in comparison to ACI, and JSCE. Furthermore, the AS relation exhibits more reliability for GFRP types than any of the chosen equations.

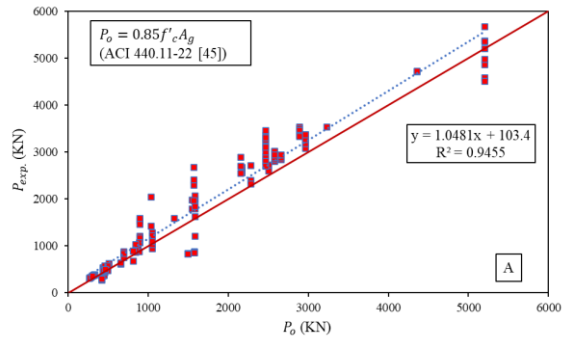

a. ACI code equation.

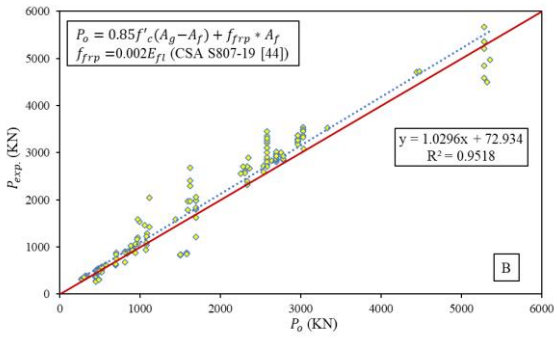

b. CSA code equation.

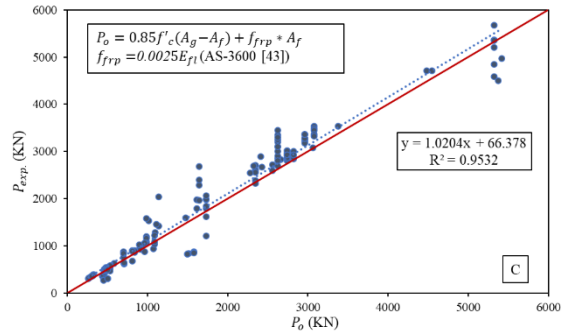

c. AS code equation.

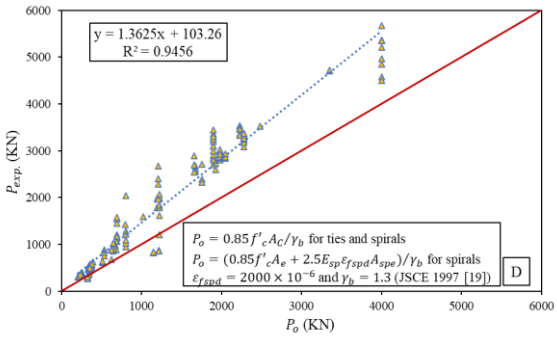

d. JSCE code equation.

Figure 1. The relationship between the experimental and predicted ALCC of concrete columns reinforced with GFRP bars.

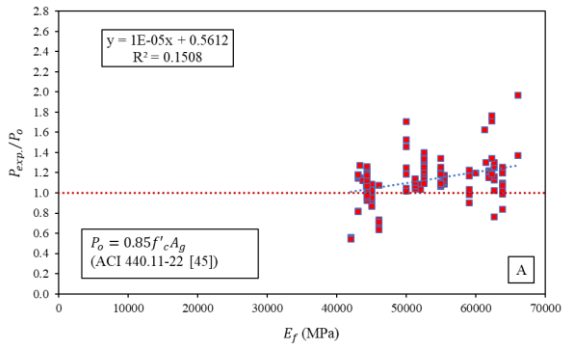

a. ACI code equation.

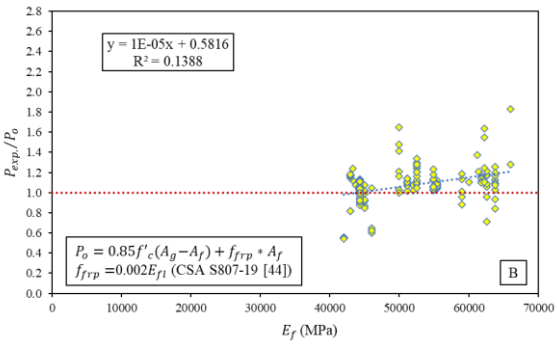

b. CSA code equation.

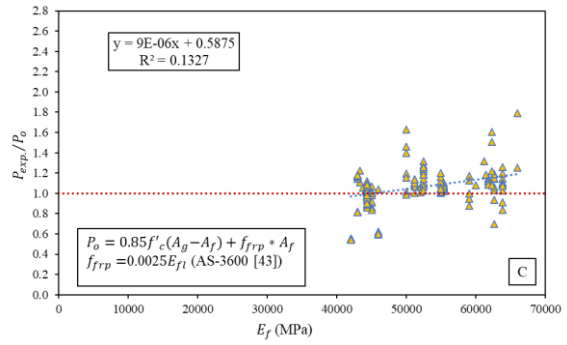

c. AS code equation.

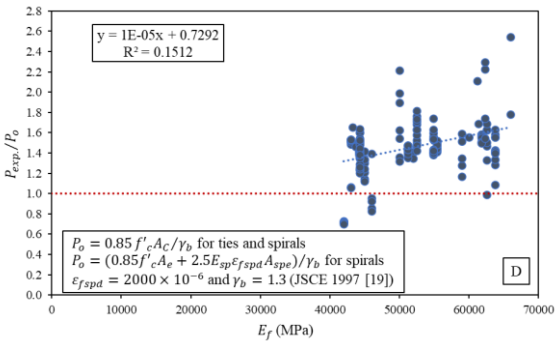

d. JSCE code equation

Figure 2. The relationship between $P_{exp.}/P_o$ of a concrete column reinforced with GFRP bars and the modulus of elasticity of the reinforcement E_f.

5.3. Compressive Strength

The ALCC of GFRP-reinforced concrete columns is majorly affected by this factor. In Fig. 3, $P_{exp.}/P_o$ is plotted against f'_c and the most optimal line trendline by the selected code equations. The ALCC for the significance of the GFRP reinforced NSC and HSC columns as mentioned in the references is over-expected by assuming ε_f= 0.0025 in (2), according to AS-3600 [43], as illustrated in Fig. 3c. The slope of the best line that gives the optimal match is -4.7E-3 in ACI, -3.8E-3 in CSA, -3.6E-3 in AS, and -6.1E-3 in JSCE. Also, the square Pearson's correlation coefficient for the ACI, CSA, AS, and JSCE have 0.111, 0.0857, 0.0801, and 0.1109, respectively. Regarding the safety of f'_c, the CSA code is safer than ACI and JSCE. In addition, AS provides the largest consistency concerning f'_c of any of the chosen code equations.

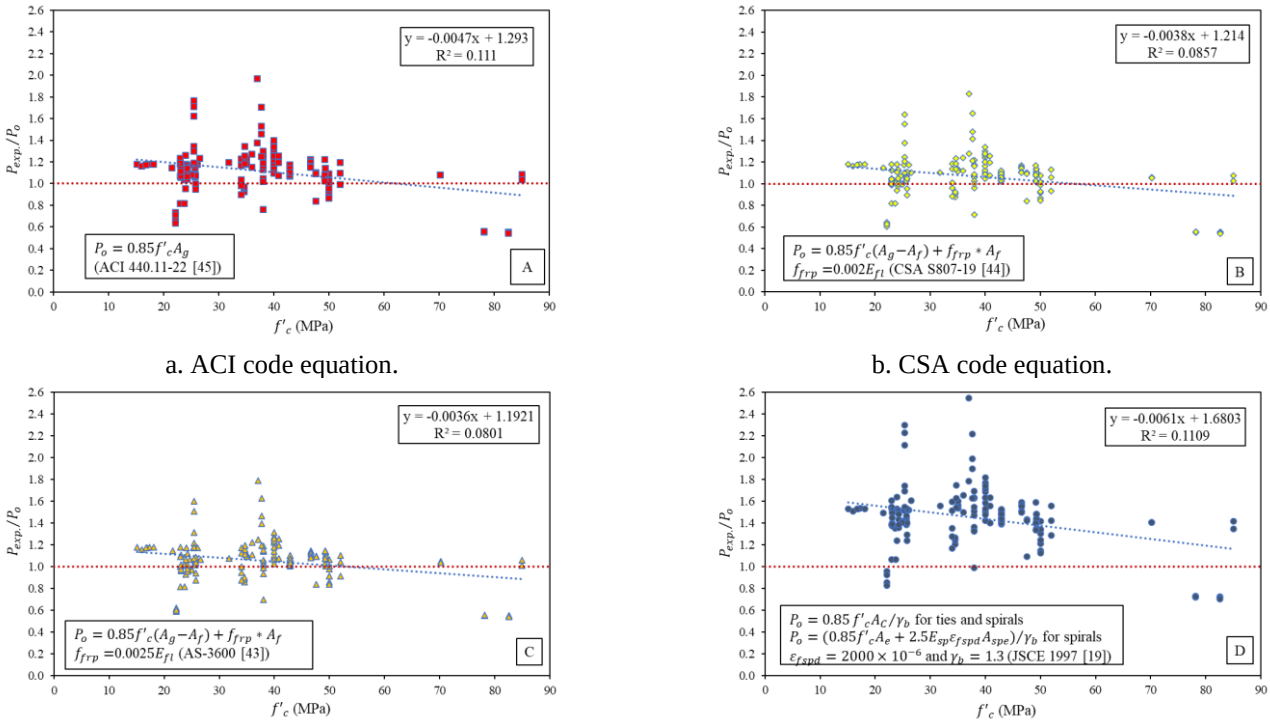

a. ACI code equation.

b. CSA code equation.

c. AS code equation.

d. JSCE code equation.

Figure 3. The relationship between $P_{exp.}/P_o$ for GFRP reinforced column with bars and the compressive strength of the concrete f'_c.

5.4. The Ratio of the Longitudinal Reinforcements.

Another necessary factor that has a large influence on the ALCC of GFRP-reinforced concrete columns is the longitudinal reinforcement ratio. The fluctuation in $P_{exp.}/P_o$ with longitudinal reinforcement ratio, according to the database, is shown in Fig. 4. The inclination of the optimal line for ACI, CSA, AS, and JSCE is 22.2E-3, -3E-3, -10.4E-3, and 25.5E-3, respectively. Also, the square Pearson's correlation coefficient for the ACI, CSA, AS, and JSCE have 0.0055, 0.0001, 0.0014, and 0.0034, respectively. Compared to ACI, and JSCE, CSA points are less packed and they are nearer to the perfect horizontal line. Concerning safety, CSA is more consistent concerning ρ_{fl} than JSCE and ACI. It can be concluded that CSA is more consistent for the GFRP type than the JSCE and ACI codes considered. Moreover, the AS's curve showed a behavior "different from the other three curves, where an increase in ρ_{fl} leads to a very close of the AS equation curve to the ideal line and thus is more stable" and provides more consistent results than the rest of the other code equations. It can be concluded that the AS relation is more consistent concerning the type of GFRP than other code relations adopted.

5.5. Transverse Reinforcement Ratio.

5.5.1 Spiral reinforcement ratio

Fig. 5 shows $P_{exp.}/\ P_o$ plotted against ρ_{ft} and the most optimal line trendline. The inclination of the optimum lines equals 39.7E-3, 36.9E-3, 36.1E-3, and 51.4E-2 for ACI, CSA, AS, and JSCE, in that order. Also, the square Pearson's correlation coefficient for the ACI, CSA, AS, and JSCE have 0.061, 0.07, 0.0718, and 0.0608, respectively. It is evident from Fig. 5 that the spiral reinforcement curve takes an upward trend in all code equations. That means that increasing distances of the spiral reinforcement within the practical limits enhance its performance [28], [49], [51], [52], [54], [56], [59,] [61], [63], [68], [72]. Also, ACI is more consistent concerning ρ_{ft} safety than JSCE and CSA. In addition, the AS code is more consistent regarding to ρ_{ft} than other codes.

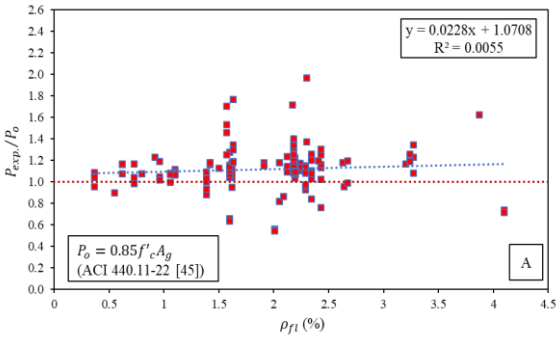

a. ACI code equation.

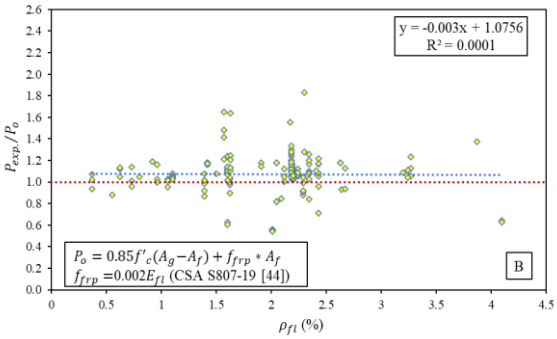

b. CSA code equation.

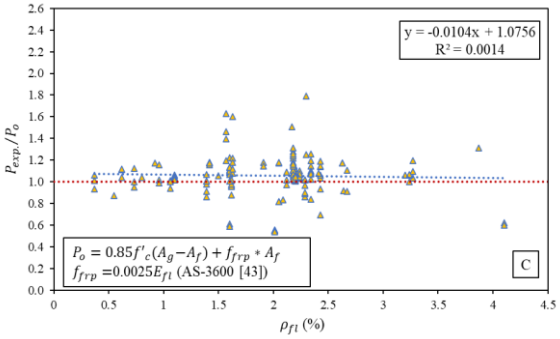

c. AS code equation.

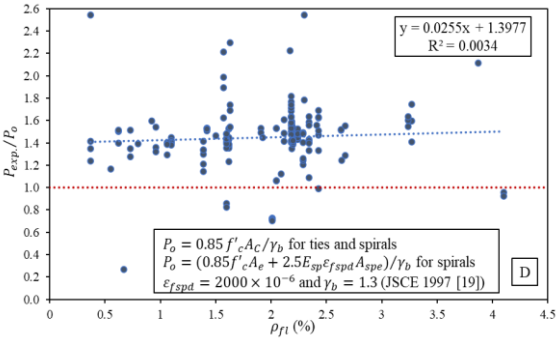

d. JSCE code equation.

Figure 4. The relationship between $P_{exp.}/P_o$ of a concrete column reinforced with GFRP bars and the longitudinal reinforcement ratio ρ_{fl}.

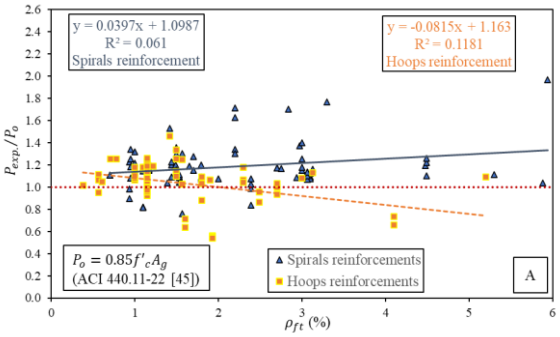

a. ACI code equation.

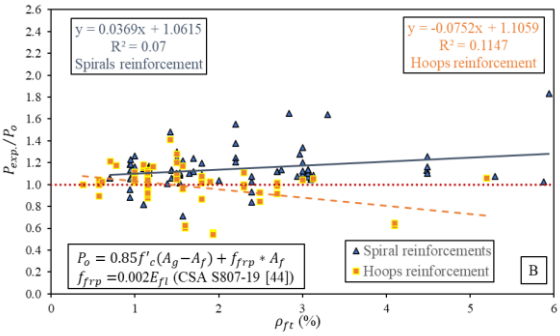

b. CSA code equation.

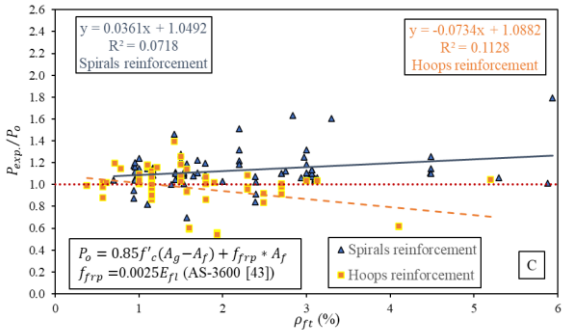

c. AS code equation.

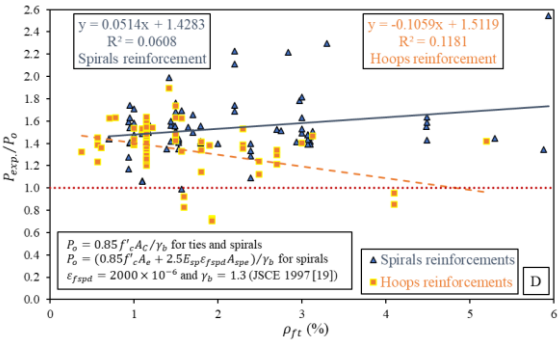

d. JSCE code equation.

Figure 5. The relationship between $P_{exp.}/P_o$ and ρ_{ft} of GFRP reinforced column.

5.5.2 Reinforcement ratio of hoops

In Fig. 5, $P_{exp.}/P_o$ is plotted against ρ_{ft} and the optimum line trendline. In ACI, CSA, AS, and JSCE, the inclination of the optimum line equals -81.5E-3, -75.2E-3, -73.4E-3, and -105.9E-3, respectively. Also, the square Pearson's correlation coefficient for the ACI, CSA, AS, and JSCE have 0.1181, 0.1147, 0.1128, and 0.1181, respectively. In general, it is evident from Fig. 5 that the curve representing the hoop reinforcement takes a downward trend in all code equations. This indicates that decreasing distances between hoops within the practical limits enhances their performance. Also, CSA safety is more consistent regarding ρ_{ft} than JSCE and ACI. In addition, AS is superior to other codes concerning ρ_{ft} consistency.

At last, the optimum line trendline behavior of spiral reinforcement is obvious, it is the adverse of the hoop reinforcement. In addition, AS and CSA present better outcomes in comparison with JSCE and ACI generally.

6. Conclusions

An extensive experimental database comprising 165 GFRP-RC columns was adopted to examine the interrelation of column details and geometry. The ALCC of the database was evaluated according to several design codes, with the AS code demonstrating superior precision compared to CSA, ACI, and JSCE. Mean factors of safety in AS, CSA, ACI, and JSCE were equal to 1.06, 1.07, 1.11, and 1.45, respectively. JSCE exhibited less consistency than AS, ACI, and CSA while disregarding the effect of longitudinal reinforcement and ultimate axial strain. Key distinctions between GFRP-RC and steel RC columns were regarded, like as varying types of GFRP (modulus of elasticity 42-66 GPa), failure in compression happened because of crushing of concrete, no yielding in GFRP reinforcements occurs nor excessive deformations. AS relation presents good compatibility with the experimental results in a comparison with the relations of other codes. That could be a remarkable conclusion because of the complexity of the GFRP behavior and the large variation of the behavior of its bars in both, tension and compression. The analysis surveys the influences of concrete compressive strength, longitudinal and transverse reinforcement ratio, and modulus of elasticity of GFRP. JSCE exhibited significantly conservative behavior, resulting in higher implementation costs. AS equation yielded the lowest COV, SD, and errors. Considering the contribution of longitudinal reinforcement enhanced reliability, accuracy, consistency, and safety for AS and CSA, unlike ACI and JSCE. Neglecting longitudinal bars and assuming fully concrete sections produced extreme values. Equations relying on longitudinal bar stiffness and associated axial strain delivered accurate, consistent, and safe results, aligning closely with experimental loads.

Acknowledgments

The authors would like to express their sincere thanks and gratitude to the Journal of Engineering and Sustainable Development (JEASD) for the support provided.

Conflict of interest

The authors declare that there are no conflicts of interest regarding the publication of this manuscript.

Author Contribution Statement

Author Hassan: proposed the research problem. Author Mohamed: developed the theory and performed the computations. Author Hassan: verified the analytical methods and supervised the findings of this work. The author Mohamed discussed the results and contributed to the final manuscript.

References

[1] F. Alhussainy, H. A. Hasan, M. N. Sheikh, and M. N. S. Hadi, “A New Method for Direct Tensile Testing of Concrete”, *J. Test. Eval.*, vol. 47, no. 2, p. 704-718, Apr. 2018, doi: https://doi.org/10.1520/jte20170067.

[2] H. A. Hasan, F. Alhussainy, M. N. Sheikhand M. N. S. Hadi, “Direct tensile test of high strength concrete with and without steel fibers”, *Mechanics of Structures and Materials XXIV*, pp. 516–521, Jun. 2019.

[3] K. Kobayashi and T. Fujisaki, “Compressive Behaviour of FRP Reinforcement in Non-Prestressed Concrete Members”, in Non-Metallic (FRP) Reinforcement for Concrete Structures: Proceedings of the Second International RILEM Symposium, pp. 42-51, Jun. 1995, DOI https://doi.org/10.1201/9781482271621-42.

[4] A. Salah-Eldin, H. M. Mohamedand B. Benmokrane, “Structural performance of high-strength concrete columns reinforced with GFRP bars and ties subjected to eccentric loads”, *Eng. Struct.*, vol. 185, pp. 286–300, Jan. 2019, doi: https://doi.org/10.1016/j.engstruct.2019.01.143.

[5] L. Sun, M. Weiand N. Zhang, “Experimental study on the behavior of GFRP reinforced concrete columns under eccentric axial load”, *Constr. Build. Mater.*, vol. 152, pp. 214–225, Jun. 2017, doi: https://doi.org/10.1016/j.conbuildmat.2017.06.159

[6] W. P. Wu, "Thermomechanical properties of Fiber Reinforced Plastic (FRP) bars", Ph.D. dissertation, West Virginia University, Morgantown, WV, USA, Jun. 1992.

[7] O. Chaallal and B. Benmokrane, “Physical and mechanical performance of an innovative glass-fiber-reinforced plastic rod for concrete and grouted anchorages”, *Can. J. Civ. Eng.*, vol. 20, no. 2, pp. 254–268, Jun. 1993, doi: https://doi.org/10.1139/l93-031.

[8] D. H. Deitz, I. E. Harikand H. Gesund, “Physical properties of glass fiber reinforced polymer rebars in compression”, *J. Compos. Constr.*, vol. 7, no. 4, pp. 363–366, Jun. 2003, doi: https://doi.org/10.1061/(ASCE)1090-0268(2003)7:4(363).

[9] A. Tavassoli, J. Liu, and S. Sheikh, "Glass fiber-reinforced polymer-reinforced circular columns under simulated seismic loads", *ACI Struct. J.*, vol. 112, no. 1, pp. 103-114, Jun. 2015, doi: https://doi.org/10.14359/51687227.

[10] L. AlNajmi and F. Abed, “Evaluation of FRP bars under compression and their performance in RC columns”, *Materials*, vol. 13, no. 20, p. 4541, Jun. 2020, doi: https://doi.org/10.3390/ma13204541.

[11] W. Xue, F. Peng, and Z. Fang, "Behavior and design of slender rectangular concrete columns longitudinally reinforced with fiber-reinforced polymer bars", ACI Struct. J., vol. 115, no. 2, pp. 311-322, Jun. 2018. doi: https://doi.org/10.14359/51701131.

[12] O. S. AlAjarmeh, A. C. Manalo, B. Benmokrane, P. V. Vijay, W. Ferdous, and P. Mendis, "Novel testing and characterization of GFRP bars in compression," *Constr. Build. Mater.*, vol. 225, pp. 1112-1126, Aug. 2019, doi: https://doi.org/10.1016/j.conbuildmat.2019.07.280.

[13] K. Khorramian and P. Sadeghian, "Material characterization of GFRP bars in compression using a new test method," *J. Test. Eval.*, vol. 49, no. 2, pp. 1037-1052, Mar. 2021, doi: https://doi.org/10.1520/JTE20180873.

[14] N. Elmessalami, A. El Refai, and F. Abed, "Fiber-reinforced polymer bars for compression reinforcement: A promising alternative to steel

bars," *Constr. Build. Mater.*, vol. 209, pp. 725-737, Mar. 2019, doi: https://doi.org/10.1016/j.conbuildmat.2019.03.105.

[15] CAN/CSA S806–R2017, Design, and Construction of Building Structures with Fibre-Reinforced Polymers, Mississauga, ON, Canada: *Canadian Standard Association*, 2012.

[16] CAN/CSA-S6-06-2019, Canadian Highway Bridge Design Code, Mississauga, ON: *Canadian Standard Association*, 2012.

[17] ACI 440.1R-06, Guide for the Design and Construction of Structural Concrete Reinforced with FRP Bars, Farmington Hills, MI, USA: *American Concrete Institute*, 2006.

[18] ACI 440.1 R-15, Guide for the Design and Construction of Structural Concrete Reinforced with FRP Bars, Farmington Hills, MI, USA: *American Concrete Institute*, 2015.

[19] Japan Society of Civil Engineers (JSCE), "Recommendation for Design and Construction of Concrete Structures Using Continuous Fiber Reinforced Materials," Concrete Engineering Series 23, *Research Committee on Continuous Fiber Reinforcing Materials*, 1997.

[20] Y. Idris and T. Ozbakkaloglu, "Seismic behavior of high-strength concrete-filled FRP tube columns," *J. Compos. Constr.*, vol. 17, no. 6, p. 04013013, Dec. 2013. doi: https://doi.org/10.1061/(ASCE)CC.1943-5614.0000388.

[21] M. N. S. Hadi, H. A. Hasan, and M. N. Sheikh, "Experimental investigation of circular high-strength concrete columns reinforced with glass fiber-reinforced polymer bars and helices under different loading conditions," *J. Compos. Constr.*, vol. 21, no. 4, pp. 04017005-1-04017005-13, Aug. 2017, doi: https://doi.org/10.1061/(ASCE)CC.1943-5614.0000784.

[22] M. Wei, L. Sun, C. Zhang, and Q. Wang, "Effect of seawater exposure on compressive behavior of concrete columns reinforced longitudinally with glass fiber reinforced polymer bars," *J. Compos. Mater.*, vol. 52, no. 17, pp. 2289-2299, Jul. 2018, doi: https://doi.org/10.1177/0021998317742957.

[23] W. Abdelazim, H. M. Mohamed, and B. Benmokrane, "Effect of slenderness ratio on the performance of concrete columns reinforced with GFRP bars and spirals," *CSCE Annual Conference, Proceedings*, pp. 1-10, Jun. 12-15, 2019, Laval, QC, Canada.

[24] B. Vijaya, S. S. Selvan, and P. Vasanthi, "Experimental investigation on the behavior of reinforced concrete column containing manufactured sand under axial compression," *Materials Today: Proceedings*, vol. 39, pp. 446-453, Mar. 2021, doi: https://doi.org/10.1016/j.matpr.2020.07.717.

[25] H. A. Hasan, M. N. Sheikh, and M. N. S. Hadi, "Maximum axial load carrying capacity of Fibre Reinforced Polymer (FRP) bar reinforced concrete columns under axial compression," *Structures*, vol. 19, pp. 227-233, Jan. 2019, doi: https://doi.org/10.1016/j.istruc.2018.12.012.

[26] N. A. Farhan, M. N. Sheikh, and M. N. S. Hadi, "Behaviour of ambient cured steel fibre reinforced geopolymer concrete columns under axial and flexural loads," *Structures*, vol. 15, pp. 184-195, Jul. 2018, doi: https://doi.org/10.1016/j.istruc.2018.07.001.

[27] A. De Luca, F. Matta, and A. Nanni, "Behavior of full-scale glass fiber-reinforced polymer reinforced concrete columns under axial load," *ACI Struct. J.*, vol. 107, no. 5, pp. 589-596, Aug. 2011, doi: https://doi.org/10.14359/51663912.

[28] M. Z. Afifi, H. M. Mohamed, and B. Benmokrane, "Strength and axial behavior of circular concrete columns reinforced with CFRP bars and spirals," *J. Compos. Constr.*, vol. 18, no. 2, p. 04013035, Apr. 2014, doi: https://doi.org/10.1061/(ASCE)CC.1943-5614.0000430.

[29] H. Tobbi, A. S. Farghaly, and B. Benmokrane, "Concrete columns reinforced longitudinally and transversally with glass fiber-reinforced polymer bars", *ACI Struct. J.*, vol. 109, no. 4, pp. 551-558, Aug. 2012, doi: https://doi.org/10.14359/51683874.

[30] H. Tobbi, A. S. Farghaly, and B. Benmokrane, "Behavior of concentrically loaded fiber-reinforced polymer reinforced concrete columns with varying reinforcement types and ratios", *ACI Struct. J.*, vol. 111, no. 2, pp. 375-386, Apr. 2014, doi: https://doi.org/10.14359/51686528.

[31] T. A. Hales, C. P. Pantelides, and L. D. Reaveley, "Experimental evaluation of slender high-strength concrete columns with GFRP and hybrid reinforcement", *J. Compos. Constr.*, vol. 20, no. 6, p. 04016050, Dec. 2016, doi: https://doi.org/10.1061/(ASCE)CC.1943-5614.0000709.

[32] M. Elchalakani and G. Ma, "Tests of glass fibre reinforced polymer rectangular concrete columns subjected to concentric and eccentric axial loading," *Eng. Struct.*, vol. 151, pp. 93-104, Aug. 2017, doi: https://doi.org/10.1016/j.engstruct.2017.08.023.

[33] J. Youssef and M. N. S. Hadi, "Axial load-bending moment diagrams of GFRP reinforced columns and GFRP encased square columns", *Constr. Build. Mater.*, vol. 135, pp. 550-564, Jan. 2017, doi: https://doi.org/10.1016/j.conbuildmat.2016.12.125.

[34] M. Guérin, H. M. Mohamed, B. Benmokrane, A. Nanni, and C. K. Shield, "Eccentric behavior of full-scale reinforced concrete columns with glass fiber-reinforced polymer bars and ties", *ACI Struct. J.*, vol. 115, no. 2, pp. 489-499, 2018, doi: https://doi.org/10.14359/51701107.

[35] M. Guérin, H. M. Mohamed, B. Benmokrane, C. K. Shield, and A. Nanni, "Effect of glass fiber-reinforced polymer reinforcement ratio on axial-flexural strength of reinforced concrete columns", *ACI Struct. J.*, vol. 115, no. 4, pp. 1049-1061, 2018, doi: https://doi.org/10.14359/51701279.

[36] A. Hadhood, H. M. Mohamed, and B. Benmokrane, "Axial load-moment interaction diagram of circular concrete columns reinforced with CFRP bars and spirals: experimental and theoretical investigations", *J. Compos. Constr.*, vol. 21, no. 2, pp. 04016092-1-04016092-12, Apr. 2017, doi: https://doi.org/10.1061/(ASCE)CC.1943-5614.0000748.

[37] A. Hadhood, H. M. Mohamed, F. Ghrib, and B. Benmokrane, "Efficiency of glass-fiber reinforced-polymer (GFRP) discrete hoops and bars in concrete columns under combined axial and flexural loads", *Compos. Part B Eng.*, vol. 114, pp. 223-236, Feb. 2017, doi: https://doi.org/10.1016/j.compositesb.2017.01.063.

[38] M. Elchalakani, G. Ma, F. Aslani, and W. Duan, "Design of GFRP-reinforced rectangular concrete columns under eccentric axial loading", *Mag. Concr. Res.*, vol. 69, no. 17, pp. 865-877, Sep. 2017, doi: https://doi.org/10.1680/jmacr.16.00437.

[39] A. Raza, Q. U. Khan, and Z. Khan, "Structural behavior of GFRP-reinforced Circular HFRC columns under concentric and eccentric loading", *Arab. J. Sci. Eng.*, vol. 46, pp. 4239-4252, May 2021, doi: https://doi.org/10.1007/s13369-020-04881-0.

[40] A. Ahmed, S. Guo, Z. Zhang, C. Shi, and D. Zhu, "A review on durability of fiber reinforced polymer (FRP) bars reinforced seawater sea sand concrete", *Constr. Build. Mater.*, vol. 256, p. 119484, May 2020, doi: https://doi.org/10.1016/j.conbuildmat.2020.119484.

[41] M. Robert and B. Benmokrane, "Combined effects of saline solution and moist concrete on long-term durability of GFRP reinforcing bars", *Constr. Build. Mater.*, vol. 38, pp. 274-284, Jan. 2013, doi: https://doi.org/10.1016/j.conbuildmat.2012.08.021.

[42] N. Elmesalami, F. Abed, and A. E. Refai, "Concrete columns reinforced with GFRP and BFRP bars under concentric and eccentric loads: experimental testing and analytical investigation," *J. Compos. Constr.*, vol. 25, no. 2, p. 04021003, Apr. 2021, doi: https://doi.org/10.1061/(ASCE)CC.1943-5614.0001115.

[43] AS 3600, Concrete Structures, Sydney, Australia: *Standards Australia*, 2018.

[44] CSA S807-19, Specification for Fibre-Reinforced Polymers (2019e), Toronto, Ontario, Canada: *Canadian Standard Association*, 2019.

[45] ACI CODE-440.11-22, Building Code Requirements for Structural Concrete Reinforced with Glass Fiber-Reinforced Polymer (GFRP) Bars—Code and Commentary, Farmington Hills, MI, USA: *American Concrete Institute*, 2022.

[46] C. P. Pantelides, M. E. Gibbons, and L. D. Reaveley, "Axial load behavior of concrete columns confined with GFRP spirals", *J. Compos. Constr.*, vol. 17, no. 3, pp. 305-313, Jun. 2013, doi: https://doi.org/10.1061/(ASCE)CC.1943-5614.0000357.

[47] M. Z. Afifi, H. M. Mohamed, and B. Benmokrane, "Axial capacity of circular concrete columns reinforced with GFRP bars and spirals", *J.*

Compos. Constr., vol. 18, no. 1, pp. 04013017-1-04013017-11, Feb. 2014, doi: https://doi.org/10.1061/(ASCE)CC.1943-5614.0000438.

[48] H. M. Mohamed, M. Z. Afifi, and B. Benmokrane, "Performance evaluation of concrete columns reinforced longitudinally with FRP bars and confined with FRP hoops and spirals under axial load", *J. Bridge Eng.*, vol. 19, no. 7, pp. 04014020-1-04014020-12, Jul. 2014, doi: https://doi.org/10.1061/(ASCE)BE.1943-5592.0000590.

[49] H. Karim, B. Noel-Gough, M. N. Sheikh, and M. N. S. Hadi, "Strength and ductility behavior of circular concrete columns reinforced with GFRP bars and helices," in Proc. FRPRCS-12/APFIS-2015 - Joint Conference of the 12th International Symposium on Fiber Reinforced Polymers for Reinforced Concrete Structures, FRPRCS 2015 and 5th Asia-Pacific Conference on Fiber Reinforced Polymers in Structures, APFIS 2015, pp. 1-6, Dec. 14-16, 2015, Nanjing, China.

[50] W. Prachasaree, S. Piriyakootorn, A. Sangsrijun, and S. Limkatanyu, "Behavior and performance of GFRP reinforced concrete columns with various types of stirrups", *Int. J. Polymer Sci.*, vol. 2015, Article ID 237231, pp. 1-9, Jun. 2015, doi: https://doi.org/10.1155/2015/237231.

[51] G. B. Maranan, A. C. Manalo, B. Benmokrane, W. Karunasena, and P. Mendis, "Behavior of concentrically loaded geopolymer-concrete circular columns reinforced longitudinally and transversely with GFRP bars", *Eng. Struct.*, vol. 117, pp. 422-436, Mar. 2016, doi: https://doi.org/10.1016/j.engstruct.2016.03.036.

[52] A. Hadhood, H. M. Mohamed, and B. Benmokrane, "Failure envelope of circular concrete columns reinforced with glass fiber-reinforced polymer bars and spirals", *ACI Struct. J.*, vol. 114, no. 6, pp. 1417-1428, Dec. 2017, doi: https://doi.org/10.14359/51689498.

[53] A. Hadhood, H. M. Mohamed, and B. Benmokrane, "Experimental study of circular high-strength concrete columns reinforced with GFRP bars and spirals under concentric and eccentric loading", *J. Compos. Constr.*, vol. 21, no. 2, p. 04016078, Apr. 2017, doi: https://doi.org/10.1061/(ASCE)CC.1943-5614.0000734.

[54] X. Zhang and Z. Deng, "Experimental study and theoretical analysis on axial compressive behavior of concrete columns reinforced with GFRP bars and PVA fibers", *Constr. Build. Mater.*, vol. 172, pp. 519-532, Apr. 2018, doi: https://doi.org/10.1016/j.conbuildmat.2018.03.237.

[55] O. S. AlAjarmeh, A. C. Manalo, B. Benmokrane, W. Karunasena, P. Mendis, and K. T. Nguyen", Compressive behavior of axially loaded circular hollow concrete columns reinforced with GFRP bars and spirals," *Constr. Build. Mater.*, vol. 194, pp. 12-23, Jan. 2019, doi: https://doi.org/10.1016/j.conbuildmat.2018.11.016.

[56] J. Tu, K. Gao, L. He, and X. Li, "Experimental study on the axial compression performance of GFRP-reinforced concrete square columns", *Adv. Struct. Eng.*, vol. 22, no. 7, pp. 1554-1565, May 2019, doi: https://doi.org/10.1177/1369433218817988.

[57] N. P. Duy, V. N. Anh, N. Minh, T. Anh, and P. A. Eduardovich, "Load-carrying capacity of short concrete columns reinforced with glass fiber reinforced polymer bars under concentric axial load", *Int. J. Eng. Adv. Technol.*, vol. 9, no. 2, pp. 1712-1719, Dec. 2019, doi: https://doi.org/10.35940/ijeat.B2372.129219.

[58] A. Tabatabaei, A. Eslami, H. M. Mohamed, and B. Benmokrane, "Compression splices of GFRP bars in unconfined and confined concrete columns", *J. Compos. Constr.*, vol. 23, no. 6, pp. 04019046-1-04019046-12, Dec. 2019, doi: https://doi.org/10.1061/(ASCE)CC.1943-5614.0000974.

[59] A. Raza and Q. U. Z. Khan, "Experimental and theoretical study of GFRP hoops and spirals in hybrid fiber reinforced concrete short columns", *Mater. Struct.*, vol. 53, no. 6, pp. 1-14, Nov. 2020, doi: https://doi.org/10.1617/s11527-020-01575-9.

[60] S. El-Gamal and O. AlShareedah, "Behavior of axially loaded low strength concrete columns reinforced with GFRP bars and spirals", *Eng. Struct.*, vol. 216, p. 110732, May 2020, doi: https://doi.org/10.1016/j.engstruct.2020.110732.

[61] M. Elchalakani, M. Dong, A. Karrech, M.S. Mohamed Ali, and J.S. Huo, "Circular concrete columns and beams reinforced with GFRP bars and spirals under axial, eccentric, and flexural loading," *J. Compos. Constr.*, vol. 24, no. 3, p. 04020008, Jun. 2020, doi: https://doi.org/10.1061/(ASCE)CC.1943-5614.0001008.

[62] M.N.S. Hadi, S. Ali, and M. Neaz Sheikh, "Experimental study of GFRP-reinforced geopolymer concrete columns under different loading conditions", *J. Compos. Constr.*, vol. 25, no. 6, p. 04021052, Dec. 2021, doi: https://doi.org/10.1061/(ASCE)CC.1943-5614.0001164.

[63] A. Elhamaymy, H.M. Mohamed, and B. Benmokrane, "Durability assessment and behavior under axial load of circular GFRP-RC piles conditioned in severe simulated marine environment", *Eng. Struct.*, vol. 249, p. 113376, Oct. 2021, doi: https://doi.org/10.1016/j.engstruct.2021.113376.

[64] A.S. Bakouregui, H.M. Mohamed, A. Yahia, and B. Benmokrane, "Axial load–moment interaction diagram of full-scale circular LWSCC columns reinforced with BFRP and GFRP bars and spirals: experimental and theoretical investigations", *Eng. Struct.*, vol. 242, pp. 112538-1-112538-16, 2021, doi: https://doi.org/10.1016/j.engstruct.2021.112538.

[65] A.S. Bakouregui, H.M. Mohamed, A. Yahia, and B. Benmokrane, "Axial load–moment interaction diagram of full-scale circular LWSCC columns reinforced with BFRP and GFRP bars and spirals: experimental and theoretical investigations", *Eng. Struct.*, vol. 242, pp. 112538-1-112538-16, May 2021, doi: https://doi.org/10.1016/j.compstruct.2021.114528.

[66] S. Ali, "Behavior of Fiber Reinforced Geopolymer Concrete Circular Columns Reinforced with GFRP Bars and GFRP Helices under Different Loading Conditions", Ph.D. dissertation, School of Civil, Mining, and Environmental Engineering, University of Wollongong, Wollongong, NSW, Australia, 2021.

[67] R. Z. Hamed and H. F. Hassan, "Structural Behavior of GFRP-RC Slender Columns Under Various Eccentricity Loading Conditions," *Civil and Environmental Engineering*, vol. 19, no. 1, pp. 1-16, 2023, doi: https://doi.org/10.2478/cee-2023-0001.

[68] M. G. Gouda, H. M. Mohamed, A. C. Manalo, and B. Benmokrane, "Behavior of Hollow Glass Fiber-Reinforced Polymer-Reinforced Concrete Columns under Axial Load: Experimental and Theoretical Investigation", *ACI Struct. J.*, vol. 119, no. 6, pp. 289-302, Nov. 2022, doi: https://doi.org/10.14359/51736117.

[69] P. Sasikumar and R. Manju, "Structural Behaviour of High Strength Concrete Columns Reinforced with Glass Fibre Reinforced Polymer Bars Under Axial Loading", *Revista Română de Materiale/Romanian Journal of Materials*, vol. 52, no. 4, pp. 412-423, 2022.

[70] C. C. Chao, I. E. Harik, and H. Gesund, "Strength of Rectangular Concrete Columns Reinforced with Fiber-Reinforced Polymer Bars", *ACI Struct. J.*, vol. 103, no. 3, pp. 452-459, Jun. 2006, doi: https://doi.org/10.14359/15324.

[71] H. J. Zadeh and A. Nanni, "Design of RC Columns Using Glass FRP Reinforcement", *J. Compos. Constr.*, vol. 17, no. 3, pp. 294-304, Jun. 2013, doi: https://doi.org/10.1061/(ASCE)CC.1943-5614.0000354.

[72] H. Karim, M. N. Sheikh, and M. N. S. Hadi, "Axial load-axial deformation behaviour of circular concrete columns reinforced with GFRP bars and helices", *Constr. Build. Mater.*, vol. 112, pp. 1147-1157, Mar. 2016, doi: https://doi.org/10.1016/j.conbuildmat.2016.02.219.

[73] K. Kumar and R. P. Saini, "Adaptive neuro-fuzzy interface system based performance monitoring technique for hydropower plants", *ISH J. Hydr. Eng.*, pp. 611-621, Aug. 2022, doi https://doi.org/10.1080/09715010.2022.2115320.

[74] N. R. Kapoor A. Kumar, A. Kumar, A. Kumar, M. A. Mohammed, K. Kumar, S. Kadry, and S. Lim, "Machine learning-based CO2 prediction for office room: A pilot study", *Wireless Communications and Mobile Computing*, vol. 2022, Article ID 9404807, pp. 1-16., Mar. 2022, doi: https://doi.org/10.1155/2022/9404807.

[75] H. Naderpour, M. Akbari, M. Mirrashid, and D.-P. N. Kontoni, "Compressive Capacity Prediction of Stirrup-Confined Concrete Columns Using Neuro-Fuzzy System", *Buildings*, vol. 12, p. 1386, Sep. 2022, doi https://doi.org/10.3390/buildings12091386.